Steel and Composite Structures, Vol. 14, No. 1 (2013) 57-71
DOI: http://dx.doi.org/10.12989/scs.2013.14.1.057

Parametric study using finite element simulation for low cycle fatigue behavior of end plate moment connection

Chemin Lim[1], Wonchang Choi*[2] and Emmett A. Sumner[3]

[1]*Shell International Exploration and Production Inc., Houston, Texas 77079, USA*
[2]*Dept. of Civil, Architectural and Environmental Engineering, North Carolina A and T State University, Greensboro, NC 27411, USA*
[3]*Dept. of Civil Engineering, North Carolina State University, Raleigh, North Carolina, USA*

(Received July 4, 2012, Revised October 30, 2012, Accepted November 13, 2012)

Abstract. The prediction of the low cycle fatigue (LCF) life of beam-column connections requires an LCF model that is developed using specific geometric information. The beam-column connection has several geometric variables, and changes in these variables must be taken into account to ensure sufficient robustness of the design. Previous research has verified that the finite element model (FEM) can be used to simulate LCF behavior at the end plate moment connection (EPMC). Three critical parameters, i.e., end plate thickness, beam flange thickness, and bolt distance, have been selected for this study to determine the geometric effects on LCF behavior. Seven FEMs for different geometries have been developed using these three critical parameters. The finite element analysis results have led to the development of a modified LCF model for the critical parameter groups.

Keywords: low cycle fatigue; end plate moment connection; finite element model

1. Introduction

In past research that is related to the investigation of the cyclic behavior of end plate moment connections (EPMCs), low cycle fatigue (LCF) behavior was observed within the connection components Sumner (2003), Kasai (2003), Garlock (2003), Ballio (1997), Shi (2007) and Pipnato (2011). The related literatures show the possibility to predict of LCF behavior of EPMCs. As the previous related research by the author Lim *et al*. (2012) was limited to a single EPMC geometric combination. Due to the numerous and various material and geometric parameters that are related to EPMCs, a study is needed that investigates the sensitivity of LCF behavior to changes in these various critical parameters. To investigate this type of sensitivity, a parametric study has been conducted using numerical (FEM) analysis. The study includes tmgkskvariations of three critical geometric properties: end-plate thickness (t_p), inner and outer pitch distances (p_f), and the connection beam flange thickness (t_f), as defined in Fig. 1. It provides detailed geometric information about the end plate.

*Corresponding author, Assistant Professor, E-mail: wchoi@ncat.edu

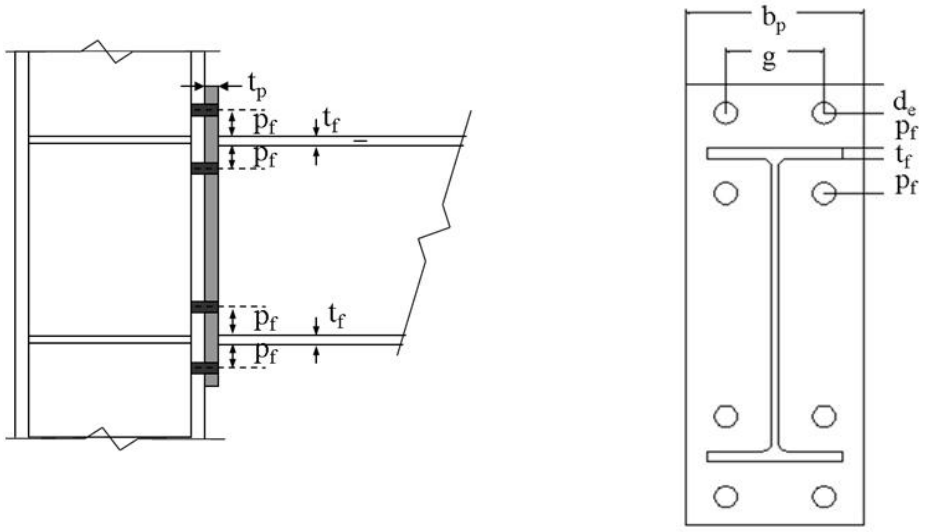

(a) Side view (b) Front view

Fig. 1 Detail geometry of end plate

The primary objectives are to investigate the effects of the identified geometric parameters on the LCF behavior of EPMCs and to apply appropriate modifications to the proposed LCF model based on the previous experimental study (Lim 2012). Eventually, the useful design method in AISC (2003) to estimate LCF of EPMC will be suggested.

The LCF effect is related primarily to the inelastic deformation of the connection (Henderson *et al*. 2009). In an EPMC, the largest inelastic deformation typically occurs in the region of the end plate beam flange connection. Three main parameters directly affect this end plate inelastic deformation: end plate thickness (t_p), beam flange thickness (t_f) and the bolt location (p_f) between the beam flange and the center of the bolt.

Numerical models were created in this study based on the original four-bolt extended unstiffened EPMC geometric parameters. As utilized in the authors study (Lim 2012), the original numerical model is designated as LCF-1-0625-2 in Table 1. The additional models were created by modifying a critical parameter for each model.

Table 1 Parametric numerical analysis matrix

Model ID	End plate THK(t_p)	Flange THK(t_f)	Bolt location(p_f)
LCF-1-0625-2 (original)	1 (25.4 mm)	0.625 (15.9 mm)	2 (50.8 mm)
LCF-075-0625-2	0.75 (19.1 mm)	0.625 (15.9 mm)	2 (50.8 mm)
LCF-125-0625-2	1.25 (31.8 mm)	0.625 (15.9 mm)	2 (50.8 mm)
LCF-1-075-2	1 (25.4 mm)	0.75 (19.1 mm)	2 (50.8 mm)
LCF-1-05-2	1 (25.4 mm)	0.5 (12.7 mm)	2 (50.8 mm)
LCF-1-0625-225	1 (25.4 mm)	0.625 (15.9 mm)	2.25 (57.2 mm)
LCF-1-0625-25	1 (25.4 mm)	0.625 (15.9 mm)	2.5 (63.5 mm)

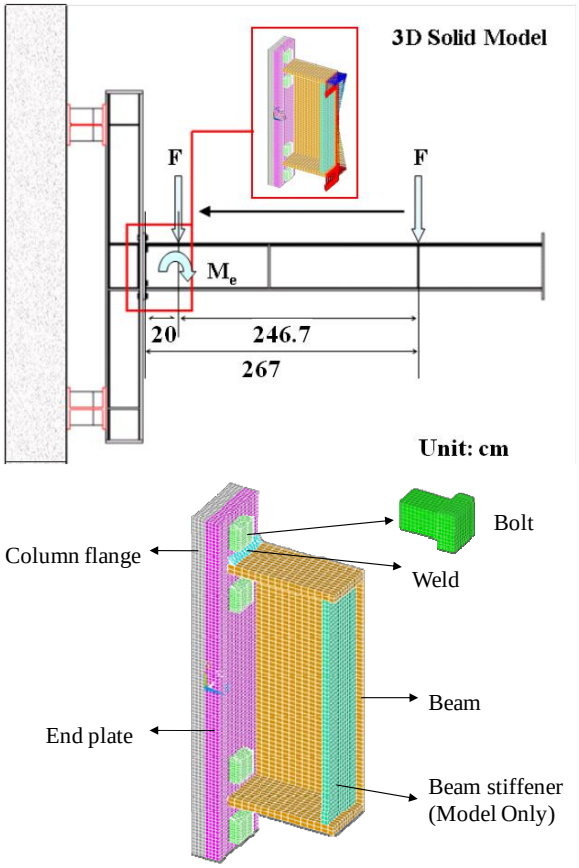

Fig. 2 Half-section 3-D FEM

2. Parametric study model

The FEM utilized in the parametric study was developed in a previous research results and literature Adany (2004), Sherbourne (1994), Bose (1997), Mays (2000), Rothert (1992), and Diaz (2011). The model was used to anticipate general behavior resulting from experimental tests. The FEM showed a good relationship with the experimental results and was used to validate the numerical results. Fig. 2 shows this previously developed three-dimensional (3D) FEM model. It was developed using a simplified half-section of a specimen that consists of four types of element: a solid element, contact element, target element, and pretension element. The simplified beam section was reduced from 267 cm to 20 cm. A stiffener was inserted at the end of the beam in this reduced section to prevent a large deformation of the beam flange. The applied load (F) was translated to an equivalent moment (M_e) and shear force (F).

The column flange, end plate, beam, and beam stiffener are defined by the SOLID45 8 nodes solid element. The weld is defined by the SOLID92 20 nodes solid element. The bolt studs are defined by SOLID45 and PREST179 to apply pretension. Two contact areas are present in the FEM. The first area is between the column flange plate and the end plate surface. The second area is between the bolt stud and the hole of the column flange and end plate. CONTA175 and

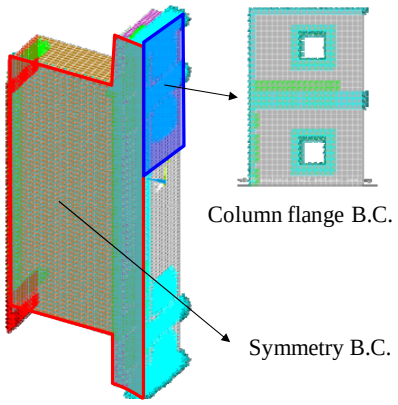

Fig. 3 Boundary conditions of FEM

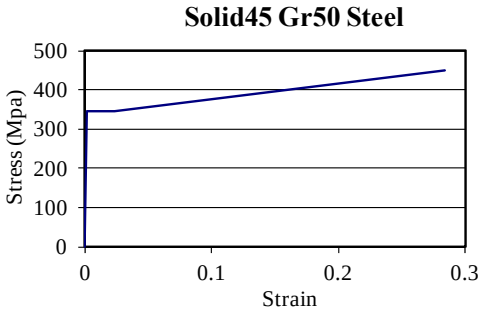

(a) Plate stress-strain curve

(b) End Plate stress-strain curve

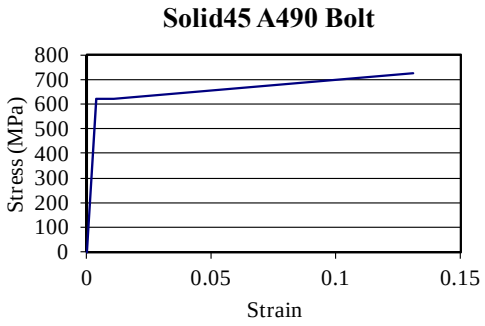

(c) Bolt stress-strain curve

Fig. 4 Element material properties

TARGE170 elements were used to define the contact condition. The mesh size is 4.76 mm, which was selected via mesh size analysis. The properties of the bolt were adjusted to take into account the rectangular shape of the bolt stud. As shown in Fig. 3, a symmetrical boundary condition was applied to the half surface. To simulate the column boundary condition, fixed boundary conditions were applied to the column flange at the column web and stiffener location. Another boundary condition is the bolt boundary condition that is a fixed boundary condition at the bottom of the stud.

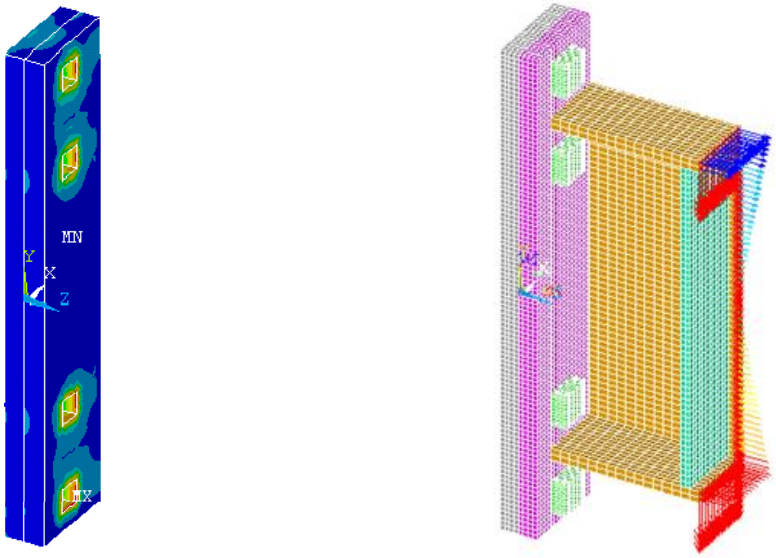

(a) Pretension force (Von Mises) (b) Applied force and pressure load

Fig. 5 Loading

Three different materials were used to develop the FEM. The beam and column were used as the measured material properties, and the bolt was adopted as a material property from previous research (Wade *et al*. 2006). To evaluate the properties of the end plate, supplementary tensile coupon tests were conducted in accordance with ASTM A370 *Standard Test Methods and Definitions for Mechanical Testing of Steel Products*. Three tension coupon samples were taken from the end plate portion that was included in the test program. An average of the stress-strain curves was derived from the three coupon tests. Fig. 4 shows the material properties of plates and bolt, respectively.

The load was applied through two steps. In the first load step, the bolt pretension force was applied with 445 kN of pretension to simulate a fully tightened moment connection. Fig. 5(a) shows the pretension deformed shape and the Von Mises stress contour. The distributed pressure was applied through the beam cross-section to apply the moment loading. Because the beam cross-section is symmetrical, the maximum pressure was applied to the top and bottom in the opposite directions. At the same time, the shear load was applied through the beam cross-section, as shown in Fig. 5(b). The maximum applied moment force was 720 kN-m.

3. Analysis of results

3.1 General behavior

The seven parametric FEMs were analyzed using the commercial code ANSYS. The models were classified into three categories based on the three critical parameters. To understand the general behavior of the connections, the Von Mises stress contour was plotted for all the parametric models at the maximum load level (720 kN-m), as shown in Fig. 6.

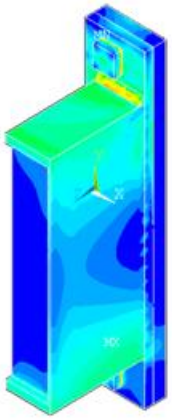

LCF-**075**-0625-2

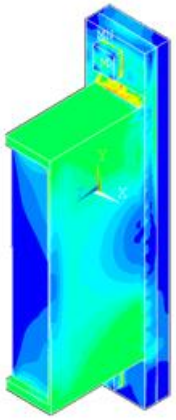

LCF-**1**-0625-2

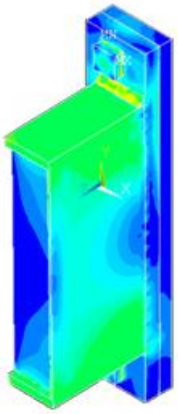

LCF-**125**-0625-2

(a) End plate thickness parameter group

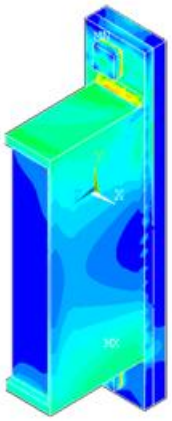

LCF-1-**05**-2

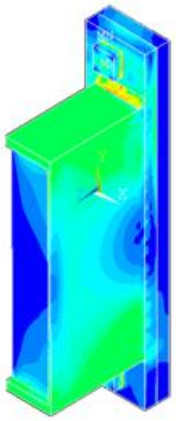

LCF-1-**0625**-2

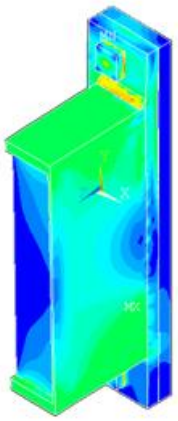

LCF-1-**075**-2

(b) Beam flange thickness parameter group

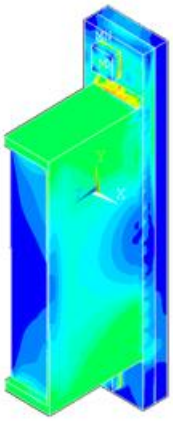

LCF-1-0625-**2**

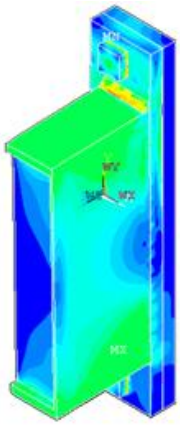

LCF-1-0625-**225**

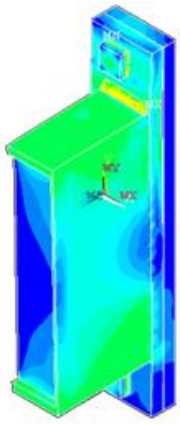

LCF-1-075-**25**

(c) Bolt distance parameter group

Fig. 6 Von-Mises stress contours

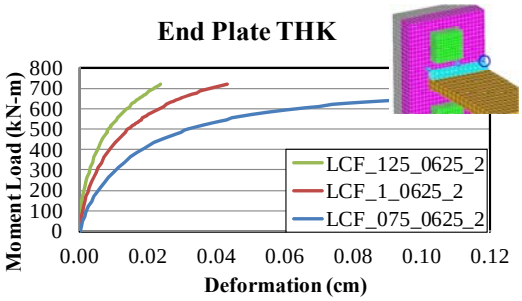

(a) End plate thickness group

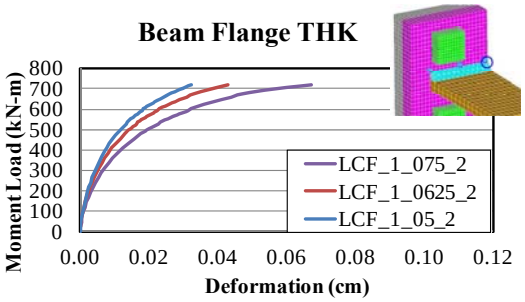

(b) Beam flange thickness group

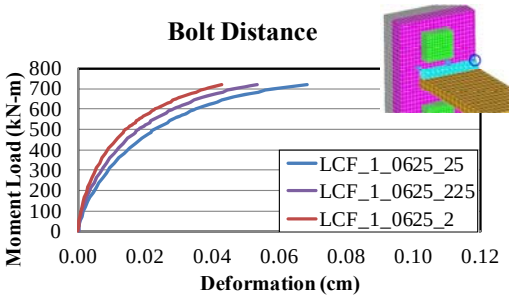

(c) Bolt distance group

Fig. 7 Out-of-plane deformations

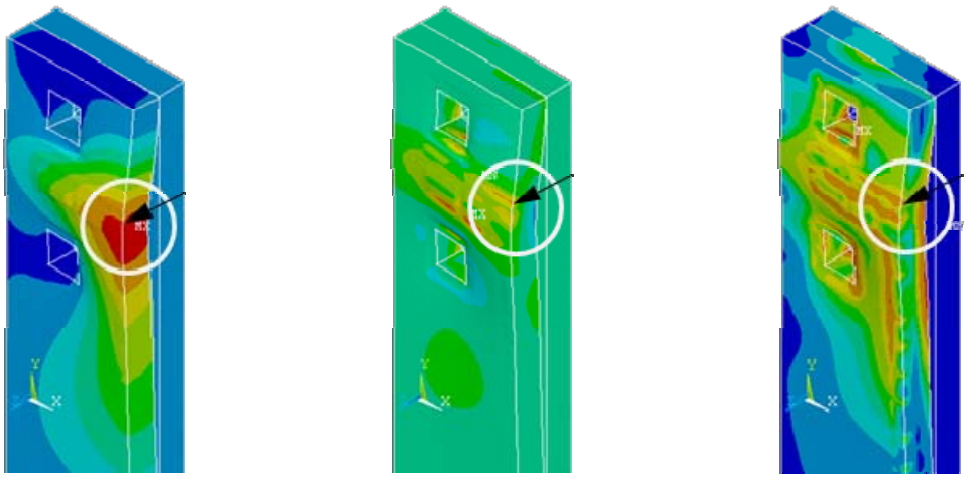

(a) Deformation (b) Longitudinal strain (c) Von-mises stress

Fig. 8 Maximum response of system (LCF-1-0635-2)

The deformation, which is the end plate out-of-plane displacement of the center of the crack point response, is plotted in Fig. 7. Overall, the FEM behaviors are reasonable.

Figs. 6 and 7 shows that all the test models exhibit a symmetrical response of the system and that the maximum stress is generated at the connection between the end plate and the beam flange.

The end plate thickness parameter group, presented in Fig. 6(a), shows that an increase of the end plate thickness generates more response from the beam and less deformation of the crack point, as indicated in Fig. 7(a). That is, a thick end plate generates a stiff response. The beam flange thickness parameter group, presented in Fig. 6(b), shows that an increase of the beam flange thickness generates performance similar to that of the end plate thickness parameter group. However, the deformation of the end plate, shown in Fig. 7(b), is smaller than the deformation for the end plate thickness group. The bolt distance parameter group, presented in Fig. 6(c), shows that a change in distance does not significantly affect beam performance. However, a longer distance creates more out-of-plane deformation, as shown in Fig. 7(c).

3.2 Local behavior

Fig. 8 presents the deformation, strain and stress contours for the original model. The figure shows that the maximum end plate out-of-plane displacement occurs at the center of the beam flange area and that a large amount of the longitudinal strain and Von Mises stress is concentrated adjacent to the weld root (Figs. 8(b) and (c)). This finding correlates well with the experimental results reported in Lim (2012), because this is the location of the LCF crack, as shown in Fig. 9(a).

In order to compare the FEM analysis results, six points were selected for each FEM. In order to determine the crack area strain level, three points were selected on the end plate along the crack line. Fig. 9(a) shows the crack levels for the actual specimen and the FEM. Another three points

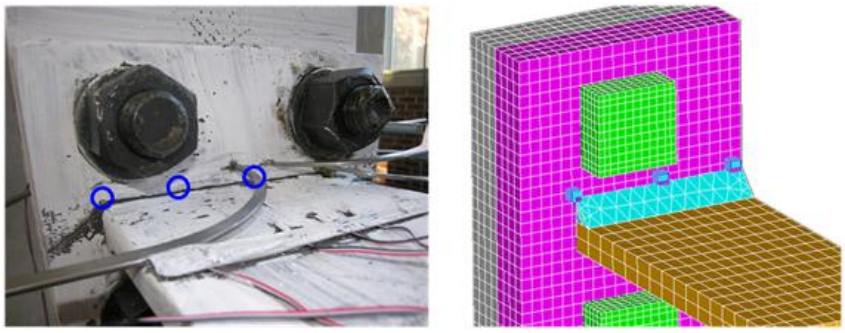

(a) End plate (crack line)

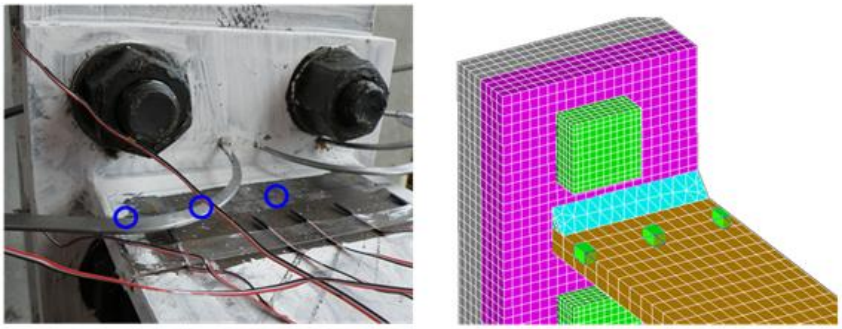

(b) Beam flange (strain gage line)

Fig. 9 FEM data collection location

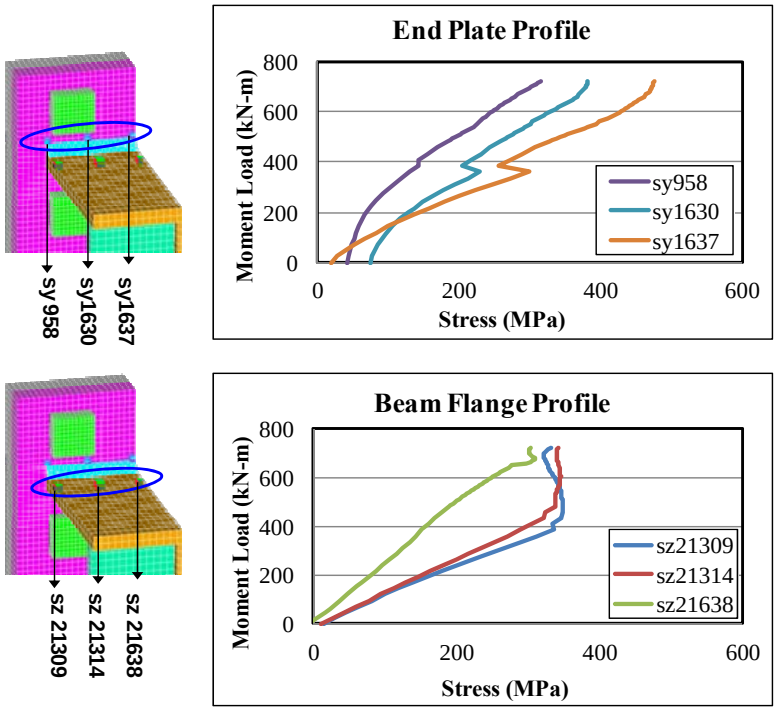

Fig. 10 Longitudinal stress results for LCF-1-0625-2

were selected on the beam flange surface at the same location where the strain gauges were installed. Fig. 9(b) shows the strain gauge and FEM.

All of the parametric study results were compared with the LCF-1-0625-2 FE model results. Fig. 9 shows selected longitudinal direction stresses and Von Mises stresses for the LCF-1-0625-2 model. Fig. 9 shows the pretension bolt effect. The 445 kN pretension was applied to each bolt, and the graph shows that the end plate did not deform until the load reached the pretension load level. Fig. 10 also shows that the center stress (measured by strain gage of sy1637) was not significantly affected by pretension due to its distance from the bolt. Both the longitudinal stress and the Von Mises stresses show similar behavior because the longitudinal stress governs the stress status. Fig. 11 shows the crack stress profile. The center of the crack line stress shows the highest value, and this point is selected as the comparison data point in this paper.

The longitudinal direction strain that is perpendicular to the crack line is used to better understand the LCF behavior, because strain results generally are used as the index for LCF fracture (Rice 1969). Therefore, all of the parametric study groups are plotted the strain along the longitudinal direction and are compared to the LCF behavior, as shown in Fig. 11. Fig. 11 shows that the top guideline is the crack line, which was observed also in the previous research program (Lim 2012). Further, the middle guideline is the weld material root and the bottom guideline is the beam flange bottom edge. The bottom guideline serves as the geometric limit of the applied loading. Although all of the model geometries are different, a large amount of strain was generated adjacent to the weld root line, as shown in Fig. 11. Fig. 11(a) shows that the thinner plate has more strain concentrated in the middle of the crack line. In Figs. 11(b) and (c), it is hard to compare the differences among the groups by the contour plot.

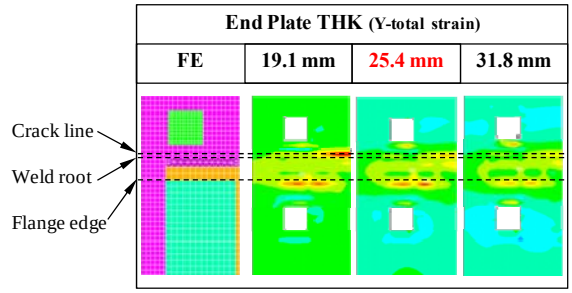

(a) End plate thickness group behavior

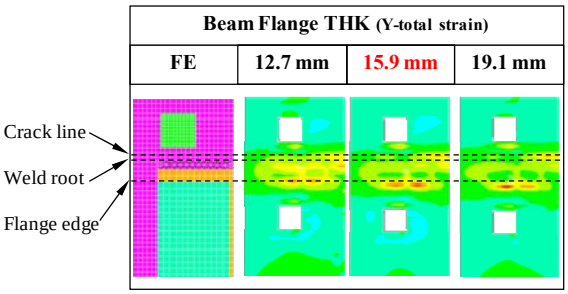

(b) Beam flange thickness group behavior

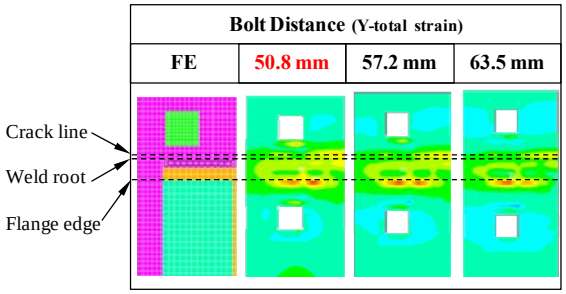

(c) Bolt distance group behavior

Fig. 11 Location of maximum strain

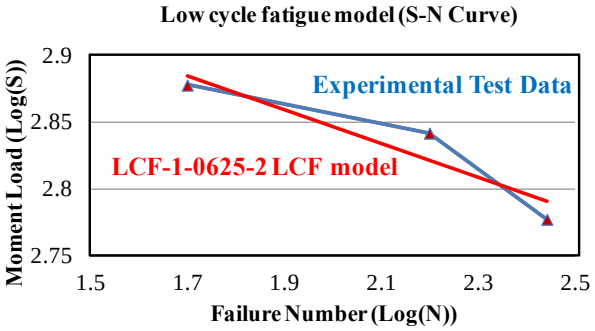

Fig. 12 LCF-1-0625-2 LCF model

4. LCF Model Modifications

The LCF model for the original parametric model (LCF-1-0625-2) was developed in a previous research program using full-scale experimental test results. Table 2 shows the summary of the previous experimental test program results that were used to generate the LCF model.

In this section, the LCF model (S-N curve) is generated using an applied moment load (S) and a failure reversal number (N) in a log-log plot. Fig. 12 shows the equivalent LCF model for LCF-1-0625-2.

However, the LCF model was developed using the stress or strain level and failure number, because the LCF crack propagation (LCF failure) is affected directly by the local stress or strain.

Table 2 LCF-1-0625-2 LCF model data

Test ID	Applied Load(*S*)	Failure No.(*N*)	log *S*	log *N*
LCF01	599 (kN.m)	276	2.777	2.441
LCF03	695 (kN.m)	158	2.842	2.199
LCF02	755 (kN.m)	50	2.878	1.699

Therefore, the strain results of the parametric studies provide the fundamental understanding of the LCF modification. As mentioned previously, the LCF model was generated using two data values: the applied moment load (S) and the failure reversal. One premise is needed to generate the modified LCF model for each parametric model. If a certain parametric model has the same longitudinal strain value as the LCF-1-0625-2 model at the center of the crack line, the level of applied loading becomes the LCF modeling data (*S*). In other words, the failure number is the same as the failure number of the LCF-1-0625-2, because a certain level of cyclic strain induces system failure with a certain number. Fig. 13 illustrates an example of the modified LCF model for the parametric tests.

The procedure for generating the modified LCF models from the parametric studies is as follows.

1. Determine the level of the constant moment loads (S1 and S2) when LCF failure occurs in the standard LCF experimental tests.
2. Determine the center of the crack positions of longitudinal strain (ε1 and ε2) from the moment-strain graph using S1 and S2 (Fig. 13(a)).
3. Determine the level of moment load (S1' and S2') from the moment-strain graph for the P1 parametric test using the ε1 and ε2 values (Fig. 13(a)).
4. Determine the failure numbers (N1 and N2) for the P1 parametric test based on the premise that the same strain level indicates the same failure number (Fig. 13(b)).
5. Plot the modified LCF model for the P1 parametric test using two data points, (log(N1), log(S1')) and (log(N2), log(S2')), in a log-log plot (Fig. 13(b)).

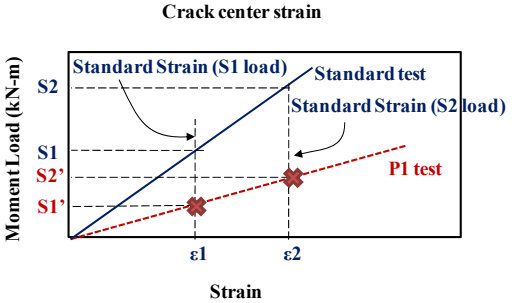

(a) End plate longitudinal strain in the center of crack line

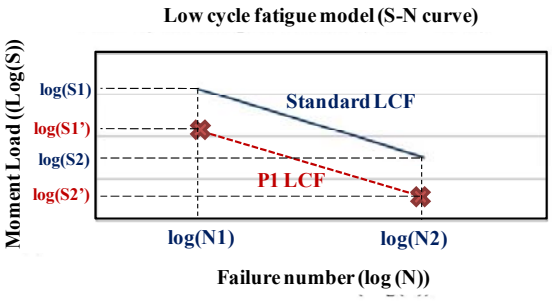

(b) Modified LCF model

Fig. 13 Modified LCF model example

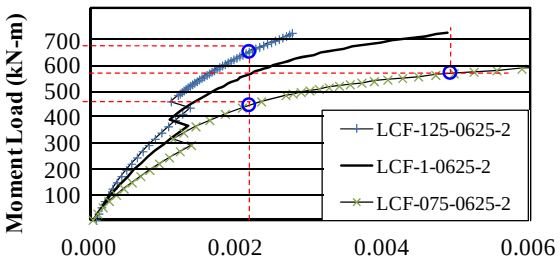

Fig. 14 End plate thickness group strain results

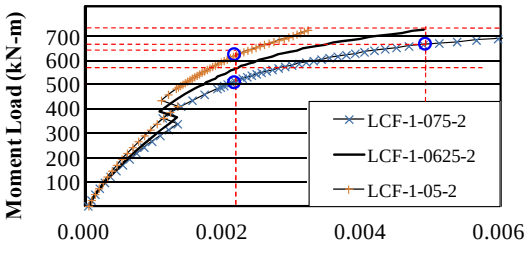

Fig. 15 End plate thickness group strain results

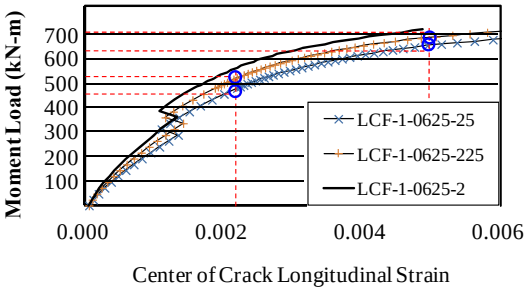

Fig. 16 Bolt distance group strain results

The longitudinal strain at the center of the crack line is plotted in Fig. 14 to 16 according to parametric group. The vertical dotted guidelines represent the level of the end plate longitudinal strains that are used to generate the LCF model. The circle indicates the cross point with the parametric strain test results and the vertical guidelines. The horizontal dotted guidelines represent the applied moment load levels for the parametric test results that have the same strain value as the LCF model strain level. The limits of strain are determined from the standard LCF model using the numerical FEM based on the constant moment load level. The lower limit of strain is 0.00256, and the higher limit of strain is 0.005.

Fig. 14 shows that the end plate thickness provides the most significant effect on the crack

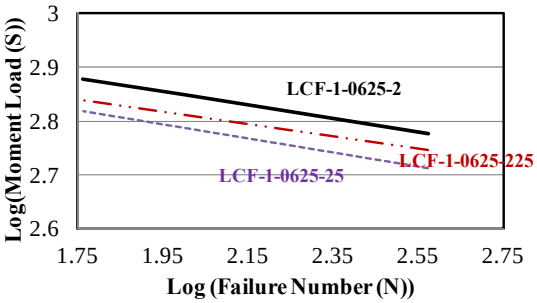

(a) End plate thickness group

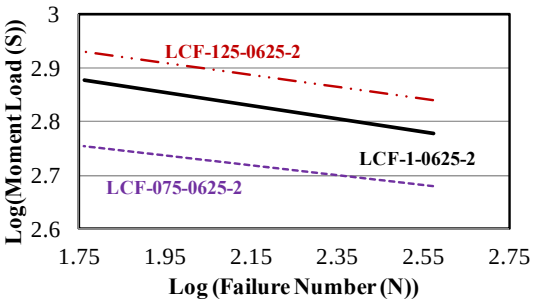

(b) Beam flange thickness group

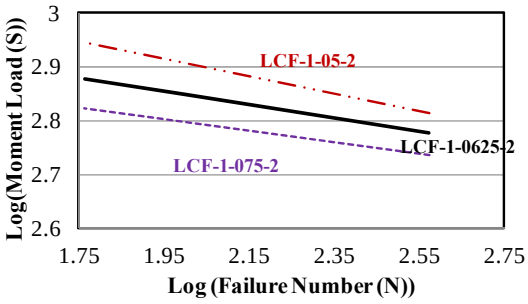

(c) Bolt distance group

Fig. 17 Modified LCF models

strain results in the parametric study. The thin plate (19 mm THK) is less stiff and has significant nonlinear behavior. The thick plate (31.7 mm THK) shows stiff behavior. However, the beam strains show almost the same behavior.

Fig. 15 shows that the beam flange thickness is less effective on the crack strain results than the end plate thickness. However, the larger flange thickness (19 mm THK) leads to more nonlinear deformation in the system. The beam strain remains almost the same until it reaches the elastic range of the material property. The thick flange (12.7 mm THK) generates the most beam strain.

Fig. 16 shows the bolt distance group and indicates that the distance between the bolt and loading position has the greatest effect on the crack strain, because more distance provides more out-of-plate deformation in the end plate, as shown in Fig. 7(c).

The LCF model can be plotted using several different load options. In this section, the y-axis S was the applied peak load However, in order to generate other geometries in the LCF models using parametric studies, the "*S*" is changed to the applied moment load. The graph is a log-log plot.

5. Conclusions

This paper presents a parametric study of the effects of three parameters: end plate thickness, beam flange thickness and bolt pitch. The study was conducted using a prequalified numerical

method. It is determined from this study that the end plate thickness is related directly to the strength of the end plate and to deformation, the beam flange thickness is related to the loading area, and the bolt distance affects the geometry of the end plate. Von Mises stress contours (Fig. 6) and maximum out-of-place deformations (Fig. 7) were used to evaluate the general behavior of the system. All of the models exhibited symmetrical behavior, and a significant stress concentration was observed at the crack line. Based on the results of the parametric studies, Different geometry connections in the LCF model can be produced using numerical analysis (FEM). The most critical parameter in the 4E EPMC is end plate thickness. The end plate thickness significantly affects both the strength of the system and the LCF model. A parametric study can be utilized to define the geometric characteristics for LCF behavior.

References

Adany, S. and Dunai, L. (2004), "Finite element simulation of the cyclic behavior of end-plate joints", *Comput. Struct.*, **82**(23-26), 2,131-2,143.

AISC, AISC Design Guide 16: Flush and Extended Multiple-Row Moment End-Plate Connections, American Institute of Steel Construction, Chicago, 2002.

American Institute of Steel Construction (AISC), *AISC Steel Design Guide 4: Extended End-Plate Moment Connections Seismic and Wind Applications*, American Institute of Steel Construction, Chicago, 2003.

American Society for Testing and Materials (ASTM), *ASTM A370-12 Standard Test Methods and Definitions for Mechanical Testing of Steel Products*, Philadelphia, PA, p. 47.

Ballio, G., Calado, L., and Castiglioni, C.A. (1997), "Low cycle fatigue behavior of structural steel members and connections", *Fatigue & Fracture of Engineering Materials & Structures*, **20**(8), 1129-1146.

Bose, B., Wang, Z.M., and Sarkar, S. (1997), "Finite-element analysis of unstiffened flush end-plate bolted joints", *J. Struct.* Eng., **123**(12), 1614-1621.

Diaz, C., Victoria, M., Marti, P. and Querin, O. (2011), "FE model of beam-to-column extended end-plate joints", J. *Constr. Steel Res.*, **67**(10), 1578-1590. http://dx.doi.org/10.1016/j.jcsr.2011.04.002.

Garlock, M.M., Ricles, J.M., and Sause, R. (2003), "Cyclic Load Tests and Analysis of Bolted Top-and-Seat Angle Connections", *J. Struct. Eng.*, **129**(12), 1615-1625.

Henderson, D.J., Ginger, J.D., Morrison, J.M. and Kopp, G.A. (2009), "Simulated tropical cyclonic winds for Low Cycle Fatigue loading of steel roofing", *Wind Struct.*, **12**(4), 381-398.

Kasai, K. and Xu, Y. (2003), "Cyclic Behavior and Low-Cycle Fatigue of Semi-Rigid Connections (Part II: Bolted T-stub Connections)", *Behaviour of Steel Structures in Seismic Areas*, STESSA 2003, Balkema, 321-327.

Lim, C., Choi, W. and Sumner, E. (2012), "Low cycle fatigue life prediction of four bolt extended unstiffened end plate moment connections", *Eng. Struct.*, **41**, 373-384

Mays, T.W. (2000), "Application of the Finite Element Method to the Seismic Design and Analysis of Large Moment End-Plate Connections", Ph.D. Dissertation, Virginia Polytechnic Institute and State University, Blacksburg, VA.

Pipinato, A., Pellegrino C. and Modena C. (2011), "Fatigue assessment of highway steel bridges in presence of seismic loading", *Eng. Struct.*, **33**(5), 1858-1858.

Rice, J. and Tracey, D. (1969), "On the ductile enlargement of voids in triaxial stress fields", *J. the Mech. Physics of Solids*, **17**(3), 201-217.

Rothert, H., Gebbeken, N. and Binder, B. (1992), "Non-linear three-dimensional finite element contact analysis of bolted connections in steel frames", *Inter. J. Numer. Methods in Eng.*, **34**(1), 303-318.

Sherbourne, A.N. and Bahaari, M.R. (1994), "3D simulation of end-plate bolted connections", *J. Struct. Eng.*, **120**(11), 3122-3136.

Shi, G.Y. and Wang, Y. (2007), "Behavior of end-plate moment connection under earthquake loading", *Eng. Struct*., **29**(5), 703-716. http://dx.doi.org/10.1016/j.engstruct.2006.06.016,

Sumner, E.A. and Murray, T.M. (2002), "Behavior of extended end-plate moment connections subject to cyclic loading", *J. Struct. Eng. ASCE*, **128**(4), 501-508.

Wade, P. (2006), "Characterization of high-strength bolt behavior in moment connections", Master's Dissertation, North Carolina State University, Raleigh, NC.

CC